Hindawi Publishing Corporation
Advances in Condensed Matter Physics
Volume 2013, Article ID 729458, 9 pages
http://dx.doi.org/10.1155/2013/729458

Research Article

The Magnetic/Electrical Phase Diagram of Cr-Doped Antiperovskite Compounds $GaCFe_{3-x}Cr_x$ ($0 \leq x \leq 0.9$)

S. Lin,[1] B. S. Wang,[1] P. Tong,[1] D. F. Shao,[1] Y. N. Huang,[1] W. J. Lu,[1] B. C. Zhao,[1] W. H. Song,[1] and Y. P. Sun[1,2]

[1] *Key Laboratory of Materials Physics, Institute of Solid State Physics, Hefei 230031, China*
[2] *High Magnetic Field Laboratory, Chinese Academy of Sciences, Hefei 230031, China*

Correspondence should be addressed to B. S. Wang; bswang@issp.ac.cn

Received 19 September 2012; Revised 13 November 2012; Accepted 20 November 2012

Academic Editor: Koshi Takenaka

We report the effect of Cr doping on the structural, magnetic, and electrical transport properties in Cr-doped antiperovskite compounds $GaCFe_{3-x}Cr_x$ ($0 \leq x \leq 0.9$). With increasing the Cr content x, the lattice constant increases while both the Curie temperature and the saturated magnetization decrease gradually. The electrical resistivity shows different behaviors as a function of x. For $x \leq 0.6$, there exists a semiconductor-like behavior below a certain temperature which decreases with increasing x. In contrast, for $0.7 \leq x \leq 0.9$, the resistivity shows a metallic behavior in the whole temperature measured (2–350 K). In particular, the Fermi-liquid behavior is obtained below 70 K. Finally, based on the magnetic and electrical properties of $GaCFe_{3-x}Cr_x$ ($0 \leq x \leq 0.9$) a magnetic/electrical phase diagram was plotted.

1. Introduction

Since $MgCNi_3$ was firstly reported as a new superconductor with the antiperovskite structure [1], the antiperovskite compounds AXM_3 (A = Ga, Al, Sn, Zn, Cu, In, Ge, Ag; X = C, N; M = Mn, Fe, Ni) have been extensively investigated [2–13]. Particularly, plenty of theoretical and experimental studies were performed for the Ni-based and Mn-based antiperovskite compounds [2–12]. Based on previous theoretical investigations [14, 15], the antiperovskite compounds AXM_3 have similar electrical band structure which determines the basical physical properties, indicating that all these antiperovskite compounds (e.g., Mn-, Fe-, or Ni-based) may exhibit similar physical properties.

Recently, considerable attention has been paid to the Fe-based antiperovskite compounds due to their interesting physical and mechanical properties, such as low temperature coefficient of resistance (LTCR) [16], magnetocaloric effect (MCE) [13, 17, 18], and good corrosion resistance [19, 20]. $GaCFe_3$ has been investigated for several decades as a typical Fe-based antiperovskite compound. It is a ferromagnetic (FM) material with the FM Curie temperature (T_C) of 510 K as reported previously [15]. Very recently, the studies of chemical doping at Ga site in $GaCFe_3$ have been reported, and some interesting physical properties such as extremely LTCR and large room-temperature MCE have been observed [13, 16, 17]. Based on the previous investigations of Mn- or Ni-based antiperovskite compounds, the chemical doping has been proved to be an effectual method to manipulate the basic physical properties [6, 10, 21–24]. As reported previously in antiperovskite compounds $GaCMn_{3-x}Ni_x$ [25], $GaCMn_{3-x}Fe$ (or Cr or Co)$_x$ [26, 27], and $SnCMn_{3-x}Fe_x$ [28], the chemical doping at Mn site can affect the magnetic and electrical transport properties significantly. Similarly, the chemical doping at Fe site for $GaCFe_3$ may be performable. However, no report was found on the chemical substitutions for the Fe site of Fe-based antiperovskite compound $GaCFe_3$. As reported previously [14, 15], the density of states at the Fermi level E_F [$N(E_F)$] is mainly from Fe 3d electrons in $AXFe_3$. As we know, the Cr ($3d^5 4s^1$) has one less 3d electron than Fe ($3d^6 4s^2$) atom. Meanwhile, the Cr atom is bigger in size than that of Fe. The influences of hole doping and the change of lattice constant on the physical properties in $GaCFe_{3-x}Cr_x$ will be thus interesting.

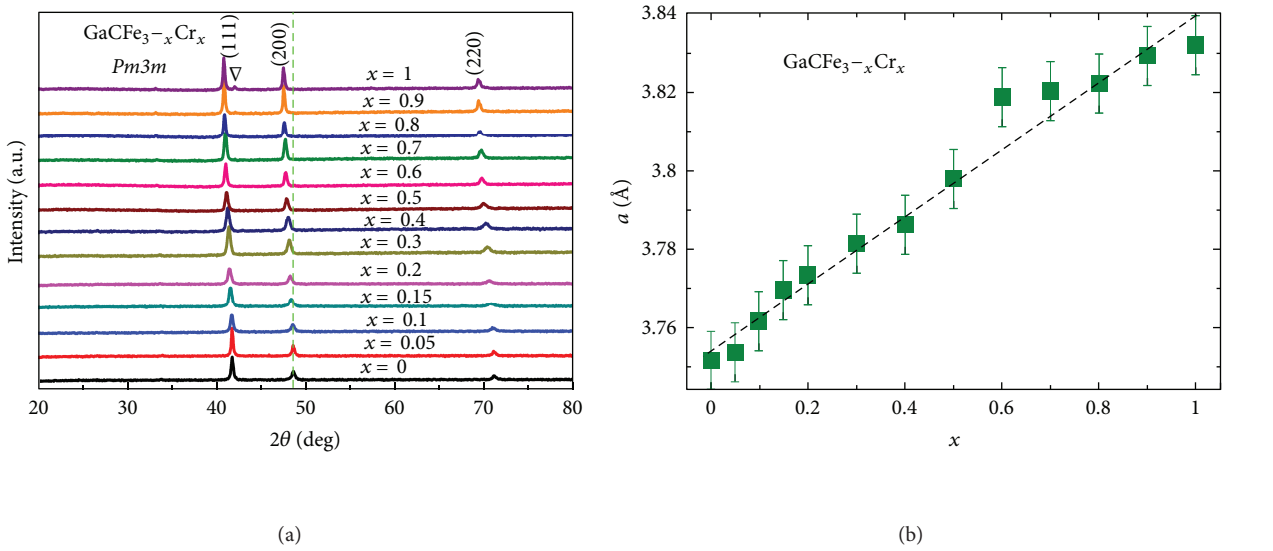

Figure 1: (Color online) (a) Room-temperature X-ray powder diffractions for $GaCFe_{3-x}Cr_x$ ($0 \le x \le 1$); the green vertical dashed line is a guide to the eye and the open triangle stands for the peak of chromium. (b) The lattice parameter a as a function of x for $GaCFe_{3-x}Cr_x$ ($0 \le x \le 1$).

In this paper, the structural, magnetic, and electrical evolutions with doping level x in $GaCFe_{3-x}Cr_x$ ($0 \le x \le 0.9$) were investigated. It is found that the lattice expands while both the Curie temperature and the saturated magnetization decrease gradually as x increases. For $GaCFe_{3-x}Cr_x$ with $x \le 0.6$, the electrical resistivity exhibits a semiconductor-like behavior at low temperature while displaying a metallic behavior at elevated temperature. As the doping level x is above 0.7, the resistivity is metallic with a T^2 temperature dependence below 70 K. Finally, a magnetic/electrical phase diagram of $GaCFe_{3-x}Cr_x$ ($0 \le x \le 0.9$) was presented.

2. Experimental Details

Polycrystalline samples $GaCFe_{3-x}Cr_x$ ($0 \le x \le 1.0$) were prepared as described in our previous paper [13]. Powder X-ray diffraction (XRD) data was collected at room temperature using an X-ray diffractometer with Cu K_α radiation (PHILIPS, $\lambda = 0.15406$ nm). The data of XRD was refined using a standard Rietveld technique to determine the crystal structure parameter and the purity of phase. Magnetic measurements were performed on a superconducting quantum interference device magnetometer (SQUID 5T, Quantum Design) and on a vibrating sample magnetometer (VSM, Quantum Design). The electrical resistivity and specific heat were carried out on a physical property measurement system (PPMS 9T, Quantum Design). The electrical transport properties were measured by the standard four-probe method to eliminate the contact resistivity.

3. Results and Discussion

Figure 1(a) shows the room-temperature XRD patterns for the samples $GaCFe_{3-x}Cr_x$ ($x = 0$, 0.05, 0.1, 0.15, 0.2, 0.3, 0.4, 0.5, 0.6, 0.7, 0.8, 0.9, and 1.0). Obviously, all $GaCFe_{3-x}Cr_x$ are single phase with a cubic antiperovskite structure (space group: $Pm3m$) except for a small amount of chromium (marked by open triangle) for $x = 1.0$. Moreover, according to the vertical bars the central position of peak (200) of $GaCFe_{3-x}Cr_x$ shifts to lower angles with an increase of Cr content, suggesting that the lattice constant expands with increasing x. The Rietveld refinements of XRD patterns were performed for all samples to determine the lattice parameter. As shown in Figure 1(b), the refined lattice parameter increases with x, which is consistent with the shift of peak (200) in Figure 1(a). The expansion of lattice can be attributed to the larger atom radius of Cr than that of Fe.

Figure 2(a) presents temperature-dependent magnetization $M(T)/M(5\,\text{K})$ curves for $GaCFe_{3-x}Cr_x$ ($0 \le x \le 0.9$) at 100 Oe under zero-field-cooled (ZFC) process. Obviously, each $M(T)$ curve exhibits an FM-PM transition as reported in $GaCFe_3$ [15]. The Curie temperature (T_C) (determined by the minimal value of dM/dT, shown in Figure 2(b)) is presented in Figure 2(d). It displays that the value of T_C decreases with increasing Cr content x. In order to investigate the magnetic ground state of $GaCFe_{3-x}Cr_x$, the isothermal $M(H)$ curves at 5 K are measured and plotted in Figure 2(c). Apparently, all the $M(H)$ curves display similar H-dependent behavior: with increasing the magnetic field, the magnetization increases initially and then tends to saturation above 10 kOe. Here, the value of saturated magnetization (M_S) is obtained by the extrapolation of the high field (10–45 kOe) $M(H)$ curve to M-axis, which is shown in Figure 2(c) (the green dash line). As shown in Figure 2(d), the M_S decreases with increasing x.

According to the previous theoretical studies [14, 15, 29], the density of states at the Fermi level E_F [$N(E_F)$] is mainly from Fe 3d electrons in $AXFe_3$. Generally, the change of $N(E_F)$ can be caused by many factors such as

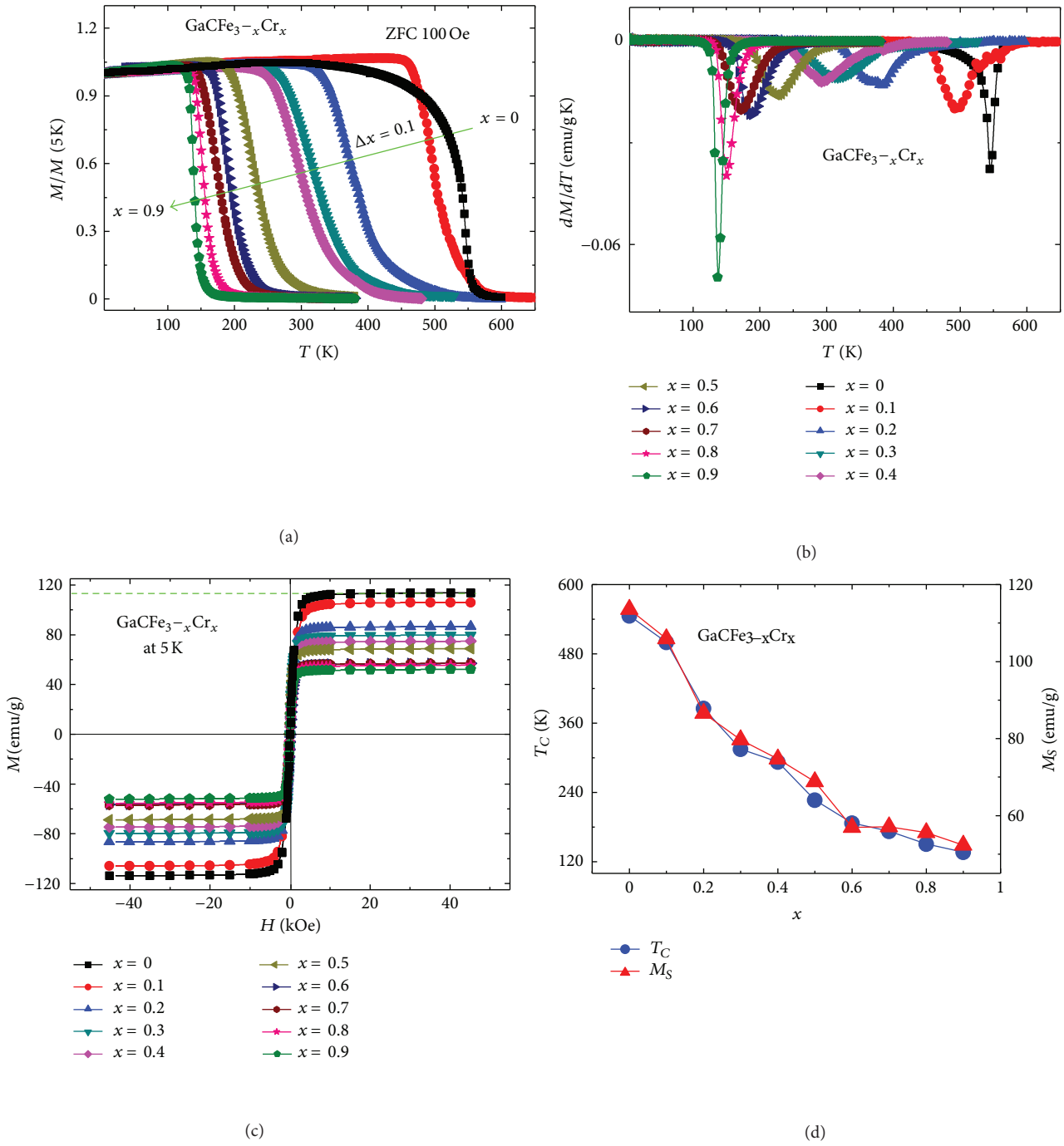

FIGURE 2: (Color online) (a) Temperature-dependent magnetization $M(T)/M(5\,\mathrm{K})$ curves under ZFC process at 100 Oe for $GaCFe_{3-x}Cr_x$ ($0 \le x \le 0.9$). (b) Temperature dependence of dM/dT for $GaCFe_{3-x}Cr_x$. (c) Magnetic field dependence of magnetization $M(H)$ curves for $GaCFe_{3-x}Cr_x$ at 5 K; inset shows the enlargement of $M(H)$ curves at positive H. (d) The x-dependent T_C and M_S for $GaCFe_{3-x}Cr_x$.

expansion/shrinkage of lattice, Fe/Cr 3d-C 2p hybridization effect, and band filling effect. In a conventional scheme, the expansion of lattice constant may give rise to the increasing of $N(E_F)$ due to the decrease of bandwidth [13, 16]. However, another important factor is associated with the detailed electronic structure at Fermi level. In $GaCFe_3$, the calculation of band structure suggests that the position of E_F is located at the left hand of a sharp peak [14]. Considering the electronic structure of Cr ($3d^5 4s^1$) and Fe ($3d^6 4s^2$), the Cr substitution for Fe can be considered as hole doping. Assuming a rigid band model, it will shift the E_F to lower energy side. As a result, the value of $N(E_F)$ in $GaCFe_{3-x}Cr_x$ is reduced with increasing x. Based on the Stoner model of itinerant ferromagnetism, the reduced

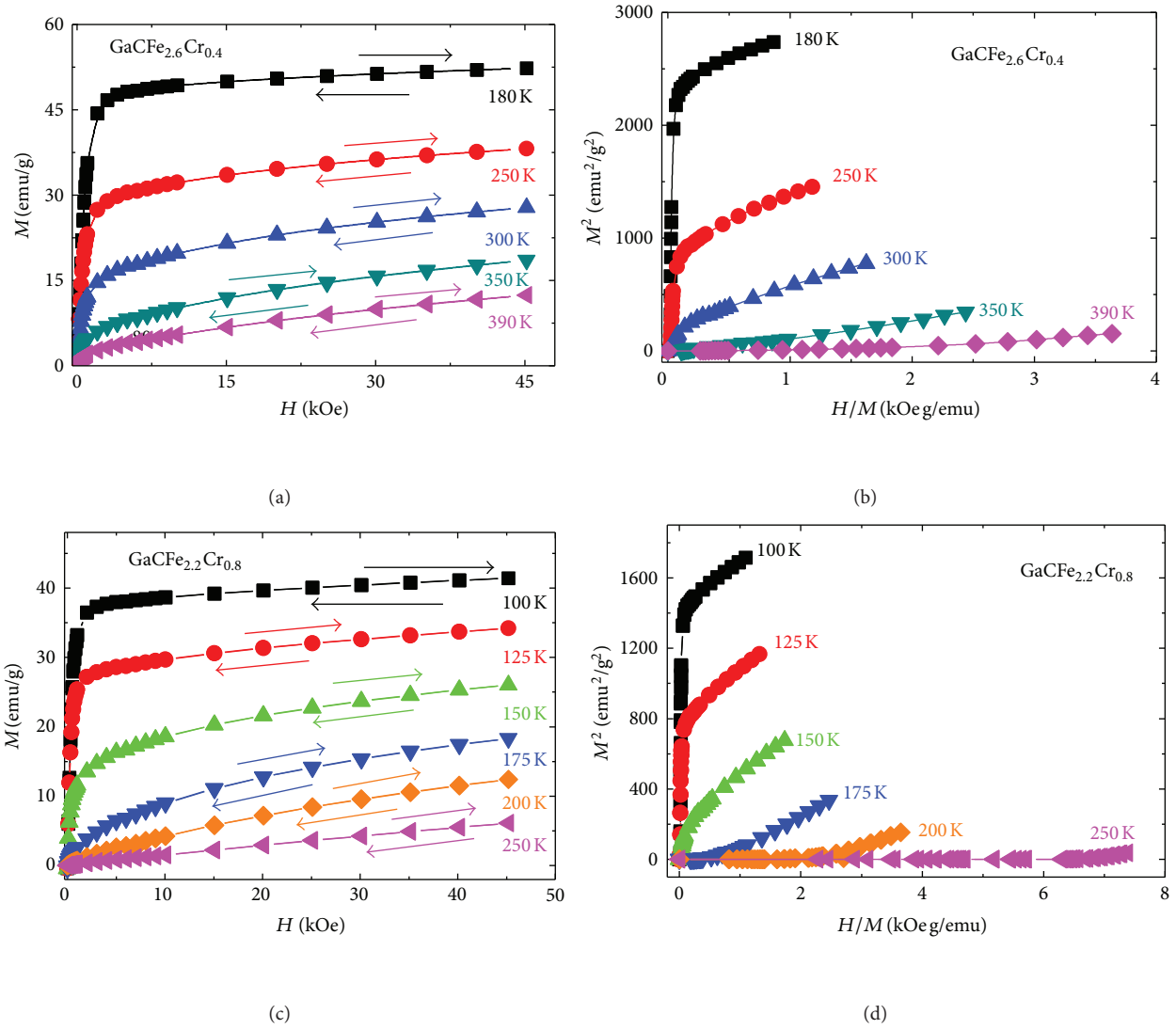

FIGURE 3: (Color online) (a) Isotherm magnetization $M(H)$ curves for $GaCFe_{2.6}Cr_{0.4}$ between 180 and 390 K with external magnetic fields up to 45 kOe. (b) The Arrott plots deduced from $M(H)$ curves in (a). (c) Isotherm magnetization $M(H)$ curves for $GaCFe_{2.2}Cr_{0.8}$ between 100 and 250 K. (d) The Arrott plots deduced from $M(H)$ curves in (c).

$N(E_F)$ will lead to a decrease in the magnetization [30]. Therefore, x-dependent M_S could be understood based on the above discussions. Now, how can the Cr-doping reduce the T_C? In itinerant ferromagnetism the main contribution to the magnetism is the itinerant electrons. Here, in $GaCFe_3$ the itinerant electrons are mainly 3d electrons of transition element. With the Cr doping level increasing, the 3d electrons decrease, which leads to a decrease in the exchange integral J. Correspondingly, the value of T_C decreases with increasing x. In a word, the evolutions of T_C and M_S are mainly attributed to the cooperation of the lattice expansion and changes of electronic structure by chemical doping.

In order to investigate the type of magnetic transition for $GaCFe_{3-x}Cr_x$, we measured the $M(H)$ curves around the corresponding T_C for the selected samples. Figure 3(a) displays the isothermal magnetization $M(H)$ curves measured between 180 and 390 K with the magnetic fields up to 45 kOe for $GaCFe_{2.6}Cr_{0.4}$. The $M(H)$ curves were measured under the increasing/decreasing field processes around T_C (~305 K). As shown in Figure 3(a), all the $M(H)$ curves around T_C are reversible during the increasing/decreasing field processes without any hysteresis, indicating a second-order magnetic transition [9]. In addition, the Arrott plots derived from $M(H)$ around T_C are presented in Figure 3(b). For $GaCFe_{2.6}Cr_{0.4}$, it is evident that the slope of H/M versus M^2 curve at high magnetic fields is positive for each temperature measured, confirming a second-order magnetic transition again [9, 23]. Analogously, for $GaCFe_{2.2}Cr_{0.8}$ ($T_C \sim 165$ K), the $M(H)$ curves and the Arrott plots in a temperature range of 100–250 K were shown in Figures 3(c) and 3(d), respectively, which confirm a second-order magnetic transition too. It is reasonable to conclude that the FM-PM transition is of second order for the left compositions in serial $GaCFe_{3-x}Cr_x$.

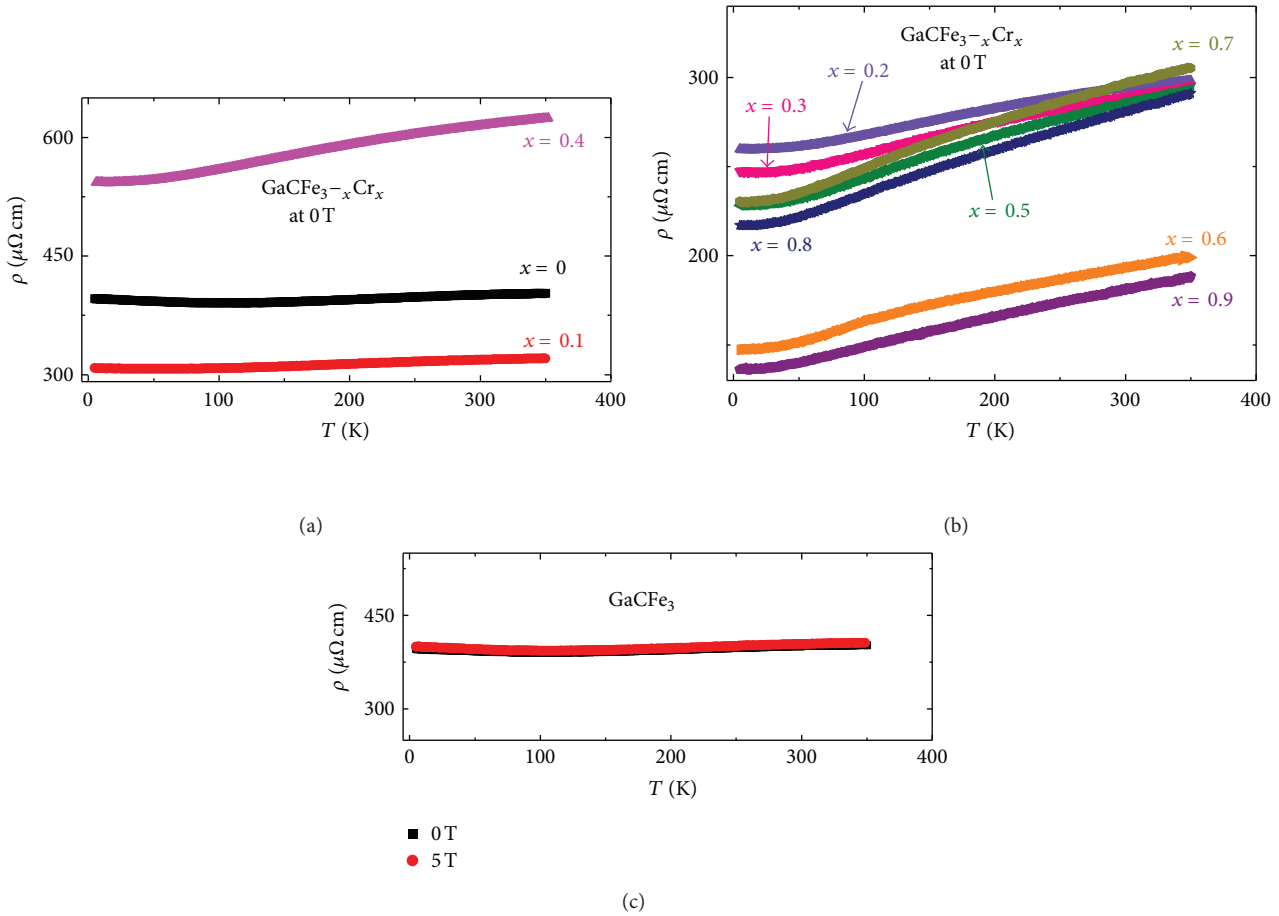

FIGURE 4: (Color online) (a)-(b) Temperature-dependent electrical resistivity at zero magnetic field in a temperature range of 2–350 K for $GaCFe_{3-x}Cr_x$ ($0 \le x \le 0.9$). (c) The resistivity as a function of temperature at zero magnetic field and 5 T for $GaCFe_3$.

Figures 4(a) and 4(b) illustrate the temperature dependence of resistivity $\rho(T)$ at zero magnetic field (2–350 K) for $GaCFe_{3-x}Cr_x$. All the magnitude of resistivity is comparable with other isostructural compounds [9, 22, 31, 32]. Figure 4(c) presents the temperature-dependent resistivity at both zero magnetic field and 5 T. Obviously, both curves are almost overlapped. The MR value (defined as $(\rho(H)-\rho(0T))/\rho(0T)$) is positive and very small ($\le 1\%$) even at 5 T, suggesting that the magnetic field has little impact on the resistivity in $GaCFe_{3-x}Cr_x$. Figure 5(a) shows the normalized resistivity $\rho(T)/\rho(350\,\text{K})$ for $GaCFe_{3-x}Cr_x$ between 2 and 350 K. There exists a minimal resistivity (ρ_{min}) and the corresponding temperature $T_{\rho_{\text{min}}}$ decreases with increasing x (to see Figure 5(b)) for low-doping samples. In high-doping samples ($0.7 \le x \le 0.9$), the ρ_{min} disappears, which can be seen clearly in Figure 5(c). As shown in Figure 5(d), the low-T resistivity was well fitted by the formula $\rho = \rho_0 + AT^2$ (ρ_0 and A represent the residual resistivity and T^2-term coefficient of the resistivity, resp.) up to about 70 K, indicating a Fermi-liquid behavior for $GaCFe_{3-x}Cr_x$ ($0.7 \le x \le 0.9$) at lower temperatures. That is to say, the electron-electron scatterings are dominant at lower temperature (5–70 K) [5, 9]. Furthermore, the fitting parameter A decreases with increasing x, which is shown in the left inset of Figure 5(d). However, at the elevated temperatures (100–270 K), $\rho(T)$ increases almost linearly with temperature for the samples with $0.7 \le x \le 0.9$ according to the fitting results (see the inset of Figure 5(c)), meaning that the contributions of electron-phonon scatterings exceed those of the electron-electron scatterings [9, 16]. In addition, the slope of linear part decreases with increasing x as displayed in the right inset of Figure 5(d). The above results can be simply understood as follows: with increasing the temperature, the number of excited phonons increases quickly, resulting in the enhancement of the phonon scatterings [9].

Figures 6(a)–6(c) show the specific heat $C_P(T)$ for $GaCFe_{3-x}Cr_x$ ($0.7 \le x \le 0.9$) measured between 7 and 70 K at zero field. As shown in the inset of Figures 6(a)–6(c), the data below 20 K is plotted as $C_P(T)/T$ versus T^2 which can be well expressed by using the following equation [5]:

$$\frac{C_P(T)}{T} = \gamma + \beta T^2 + \delta T^4, \quad (1)$$

where γ (Sommerfeld constant) is the electronic contribution, β is the phonon contribution, and δ is deviations from

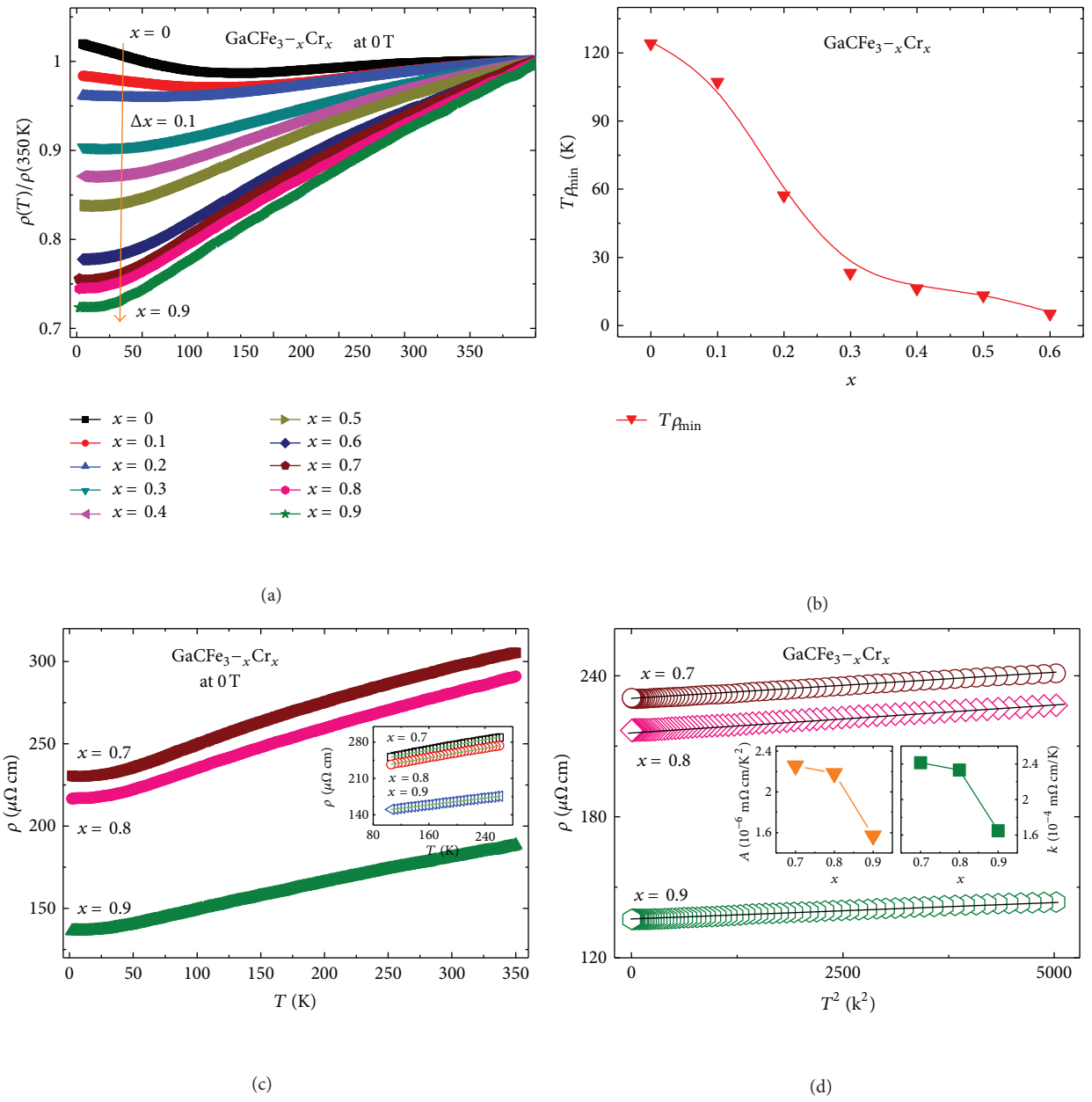

FIGURE 5: (Color online) (a) The normalized resistivity $\rho(T)/\rho(350\,\mathrm{K})$ dependence of temperature at zero field between 2 and 350 K for $GaCFe_{3-x}Cr_x$ ($0 \le x \le 0.9$). (b) The temperature of minimal resistivity as a function of x for $GaCFe_{3-x}Cr_x$ ($0 \le x \le 0.6$). (c) Temperature dependence of resistivity at zero magnetic field for $GaCFe_{3-x}Cr_x$ ($0.7 \le x \le 0.9$); inset displays the linear fits of $\rho(T)$ for the samples with $0.7 \le x \le 0.9$ between 100 and 270 K. (d) The lower-T $\rho(T)$ data plotted as $\rho(T)$ versus T^2 for the samples with $0.7 \le x \le 0.9$; the left and right insets show fitted parameters A and k as a function of x, respectively (see text for details).

TABLE 1: The fitting parameters of ρ_0, A, γ, β, σ, and Θ_D for $GaCFe_{3-x}Cr_x$ ($0.7 \le x \le 0.9$), respectively.

$GaCFe_{3-x}Cr_x$	ρ_0 ($\mu\Omega$cm)	A (10^{-6} mΩcm/K^2)	γ (mJ/mol K^2)	β (mJ/mol K^4)	σ (mJ/mol K^6)	Θ_D (K)
$x = 0.7$	239	2.26	76.3	0.046	3.66×10^{-4}	593
$x = 0.8$	217	2.18	79.3	0.071	2.99×10^{-4}	517
$x = 0.9$	136	1.57	81.7	0.085	2.79×10^{-4}	487

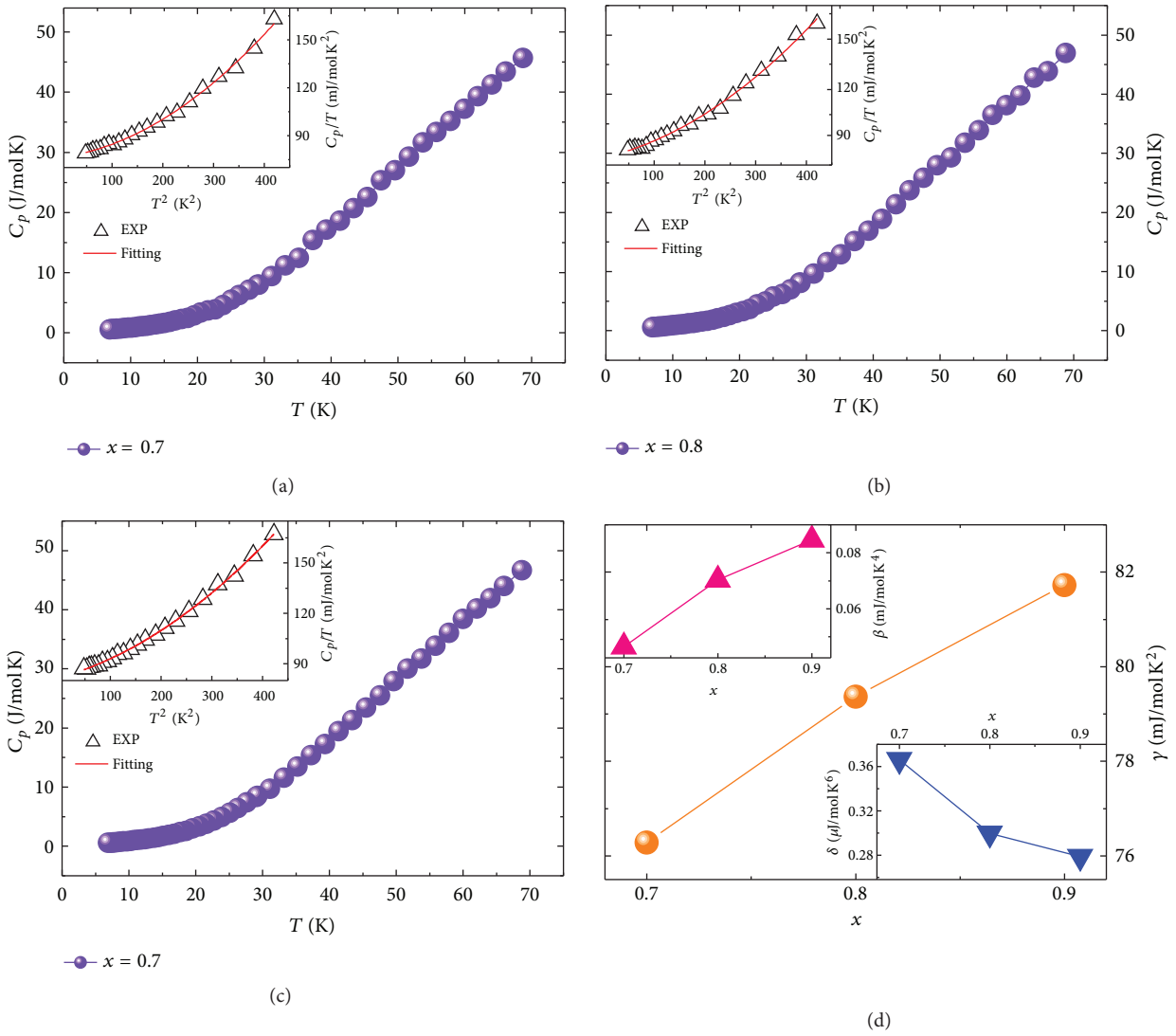

FIGURE 6: (Color online) (a)–(c) Temperature-dependent heat capacity $C_P(T)$ at zero magnetic field for $GaCFe_{3-x}Cr_x$ ($0.7 \le x \le 0.9$) between 6.7 and 70 K; inset shows the plots of $C_P(T)/T$ versus T^2 below 20 K and the solid line represents the fitting results according to (1). (d) The fitting parameter γ as a function of x for $GaCFe_{3-x}Cr_x$; the left and right insets show the parameters β and δ as a function of x, respectively.

the linear dispersion of the acoustic modes in extended temperature range. The fitted parameters γ, β, and δ as a function of x are shown in Figure 6(d) and the insets of Figure 6(d), respectively. With x increasing, the γ and β increase while the δ decreases. Accordingly, the Debye temperature $\Theta_D = ((n \times 1.94 \times 10^6)/\beta)^{1/3}$ (where n is the number of atoms in a unit cell and equal to 5 for $GaCFe_{3-x}Cr_x$ ($0.7 \le x \le 0.9$)) is derived from the value of coefficient β. The detailed results of ρ_0, A, γ, β, δ, and Θ_D for $GaCFe_{3-x}Cr_x$ ($0.7 \le x \le 0.9$) are summarized in Table 1. Generally, the value of Kadowaki-Woods (KW) ratio A/γ^2 is the well-known measure of electron-electron correlation [3, 16]. By taking the values of A and γ listed in Table 1, the KW ratio was calculated for $GaCFe_{3-x}Cr_x$ ($0.7 \le x \le 0.9$). For $x = 0.7$, 0.8, and 0.9 the values of KW ratio are 2.70×10^{-7} $\mu\Omega$ cm/(mJ/mol K)^2, 3.46×10^{-7} $\mu\Omega$ cm/(mJ/mol K)^2, and 2.38×10^{-7} $\mu\Omega$ cm/(mJ/mol K)^2, respectively, which are much less than the universal value $a_0 = 10^{-5}$ $\mu\Omega$ cm/(mJ/mol K)^2 of for strong electron-electron system [3], meaning a weak electron-electron correlation.

Finally, based on the data of magnetic and electrical transport properties, the magnetic/electrical phase diagram for $GaCFe_{3-x}Cr_x$ ($0 \le x \le 0.9$) is plotted in Figure 7. As for the magnetic phase diagram there are FM and PM regions; and the metallic, semiconducting, and Fermi-liquid areas are shown in electrical phase diagram.

4. Conclusion

In summary, we present the magnetic/electrical phase diagram of $GaCFe_{3-x}Cr_x$ ($0 \le x \le 0.9$). The influences of the Cr doping on the structure, magnetic, and electrical transport properties have been investigated systematically. With increasing the Cr content x, the lattice parameter increases while both the T_C and M_S decrease gradually. For the samples with $x \le 0.6$, the resistivity curves show a

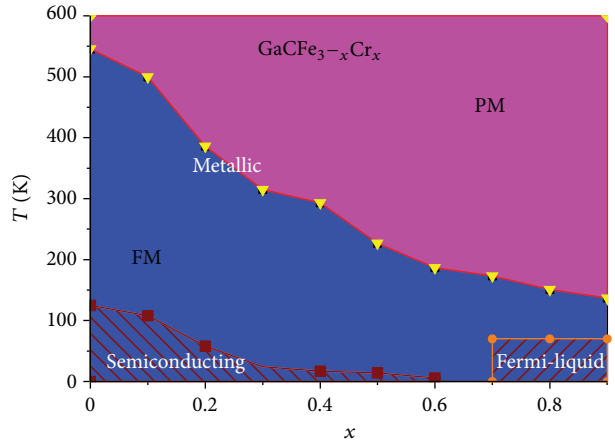

FIGURE 7: (Color online) The magnetic/electrical phase diagram for $GaCFe_{3-x}Cr_x$ ($0 \le x \le 0.9$).

semiconductor-like behavior below a certain temperature, which decreases as x increases. On the contrary, for $x \ge 0.7$ the semiconductor-like behavior disappears, and the metallic behavior is dominant in the whole temperature range (2–350 K). Particularly, the samples with $x \ge 0.7$ show a Fermi-liquid behavior at low temperatures. In addition, we confirm that the FM-PM transition in the serial $GaCFe_{3-x}Cr_x$ is of second order.

Acknowledgments

This work was supported by the National Key Basic Research under Contract no. 2011CBA00111 and the National Natural Science Foundation of China under Contracts nos. 51001094, 51171177, 11174295, and 91222109.

References

[1] T. He, Q. Huang, A. P. Ramirez et al., "Superconductivity in the non-oxide perovskite $MgCNi_3$," *Nature*, vol. 411, no. 6833, pp. 54–56, 2001.

[2] Y. B. Li, W. F. Li, W. J. Feng, Y. Q. Zhang, and Z. D. Zhang, "Magnetic, transport and magnetotransport properties of $Mn_{3+x}Sn_{1-x}C$ and $Mn_3Zn_ySn_{1-y}C$ compounds," *Physical Review B*, vol. 72, no. 2, Article ID 024411, 8 pages, 2005.

[3] P. Tong, Y. P. Sun, X. B. Zhu, and W. H. Song, "Strong electron-electron correlation in the antiperovskite compound $GaCNi_3$," *Physical Review B*, vol. 73, no. 24, Article ID 245106, 5 pages, 2006.

[4] P. Tong, Y. P. Sun, X. B. Zhu, and W. H. Song, "Strong spin fluctuations and possible non-Fermi-liquid behavior in $AlCNi_3$," *Physical Review B*, vol. 74, no. 22, Article ID 224416, 7 pages, 2006.

[5] P. Tong, Y. P. Sun, B. C. Zhao, X. B. Zhu, and W. H. Song, "Influence of carbon concentration on structural, magnetic and electrical transport properties for antiperovskite compounds AlC_xMn_3," *Solid State Communications*, vol. 138, no. 2, pp. 64–67, 2006.

[6] B. S. Wang, P. Tong, Y. P. Sun et al., "Enhanced giant magnetoresistance in Ni-doped antipervoskite compounds $GaCMn_{3-x}Ni_x (x = 0.05, 0.10)$," *Applied Physics Letters*, vol. 95, no. 22, Article ID 222509, 2009.

[7] B. S. Wang, P. Tong, Y. P. Sun et al., "Reversible room-temperature magnetocaloric effect with large temperature span in antiperovskite compounds $Ga_{1-x}CMn_{3+x}$ ($x = 0, 0.06, 0.07$, and 0.08)," *Journal of Applied Physics*, vol. 105, no. 8, Article ID 083907, 5 pages, 2009.

[8] B. S. Wang, P. Tong, Y. P. Sun et al., "Observation of spin-glass behavior in antiperovskite compound $SnCFe_3$," *Applied Physics Letters*, vol. 97, no. 4, Article ID 042508, 3 pages, 2010.

[9] B. S. Wang, J. C. Lin, P. Tong et al., "Structural, magnetic, electrical transport properties, and reversible room-temperature magnetocaloric effect in antipervoskite compound $AlCMn_3$," *Journal of Applied Physics*, vol. 108, no. 9, Article ID 093925, 6 pages, 2010.

[10] K. Takenaka and H. Takagi, "Giant negative thermal expansion in Ge-doped anti-perovskite manganese nitrides," *Applied Physics Letters*, vol. 87, no. 26, Article ID 261902, 3 pages, 2005.

[11] K. Takenaka, K. Asano, M. Misawa, and H. Takagi, "Negative thermal expansion in Ge-free antiperovskite manganese nitrides: tin-doping effect," *Applied Physics Letters*, vol. 92, no. 1, Article ID 011927, 3 pages, 2008.

[12] E. O. Chi, W. S. Kim, and N. H. Hur, "Nearly zero temperature coefficient of resistivity in antiperovskite compound $CuNMn_3$," *Solid State Communications*, vol. 120, no. 7-8, pp. 307–310, 2001.

[13] S. Lin, B. S. Wang, J. C. Lin et al., "Composition dependent-magnetocaloric effect and low room-temperature coefficient of resistivity study of iron-based antiperovskite compounds $Sn_{1-x}Ga_xCFe_3$ ($0 \le x \le 1.0$)," *Applied Physics Letters*, vol. 99, no. 17, Article ID 172503, 3 pages, 2011.

[14] A. L. Ivanovskiı, R. F. Sabiryanov, and A. N. Skazkin, "Band structure and magnetic properties of M3M'C antiperovskites (M = Mn, Fe; M′ = Zn, Al, Ga, Sn)," *Physics of the Solid State*, vol. 40, no. 9, pp. 1516–1519, 1998.

[15] F. Grandjean and A. Gerard, "Study by Mossbauer spectroscopy of the series of perovskite carbides $M_3M'C$ with M = Fe or Mn, and M′ = Al, Ga, Ge, Zn, Sn," *Journal of Physics F*, vol. 6, no. 3, pp. 451–467, 1976.

[16] S. Lin, B. S. Wang, J. C. Lin et al., "The magnetic, electrical transport and thermal transport properties of Fe-based antiperovskite compounds ZnC_xFe_3," *Journal of Applied Physics*, vol. 110, no. 8, Article ID 083914, 8 pages, 2011.

[17] S. Lin, B. S. Wang, J. C. Lin et al., "Tunable room-temperature zero temperature coefficient of resistivity in antiperovskite compounds $Ga_{1-x}CFe_3$ and $Ga_{1-y}Al_yCFe_3$," *Applied Physics Letters*, vol. 101, no. 1, Article ID 011908, 4 pages, 2012.

[18] S. Lin, B. S. Wang, X. B. Hu et al., "The structural, magnetic, electrical/thermal transport properties and reversible magnetocaloric effect in Fe-based antipervoskite compound $AlC_{1.1}Fe_3$," *Journal of Magnetism and Magnetic Materials*, vol. 324, no. 20, pp. 3267–3271, 2012.

[19] T. Takahashi, D. Music, and J. M. Schneider, "γ'-$ZnFe_3N$ thin films: a proposal for a moderately ductile, corrosion-protective coating on steel," *Scripta Materialia*, vol. 65, no. 5, pp. 380–383, 2011.

[20] D. Music and J. M. Schneider, "Elastic properties of MFe_3N (M = Ni, Pd, Pt) studied by ab initio calculations," *Applied Physics Letters*, vol. 88, no. 3, Article ID 031914, 3 pages, 2006.

[21] R. J. Huang, L. F. Li, F. S. Cai, X. D. Xu, and L. H. Qian, "Low-temperature negative thermal expansion of the antiperovskite manganese nitride Mn_3CuN codoped with Ge and Si," *Applied Physics Letters*, vol. 93, no. 8, Article ID 081902, 3 pages, 2008.

[22] K. Takenaka, A. Ozawa, T. Shibayama, N. Kaneko, T. Oe, and C. Urano, "Extremely low temperature coefficient of resistance in antiperovskite $Mn_3Ag_{1-x}Cu_xN$," *Applied Physics Letters*, vol. 98, no. 2, Article ID 022103, 3 pages, 2011.

[23] D. Fruchart and E. F. Bertaut, "Magnetic studies of the metallic perovskite-type compounds of manganese," *Journal of the Physical Society of Japan*, vol. 44, pp. 781–791, 1978.

[24] R. S. de Figueiredo, C. A. Kuhnen, and A. V. Dos Santos, "Crystallographic, magnetic and electronic structure of iron-silver and iron-gold perovskite nitrides," *Journal of Magnetism and Magnetic Materials*, vol. 173, no. 1-2, pp. 141–154, 1997.

[25] B. S. Wang, P. Tong, Y. P. Sun et al., "Structural, magnetic properties and magnetocaloric effect in Ni-doped antiperovskite compounds $GaCMn_{3-x}Ni_x$ ($0 \le x \le 0.10$)," *Physica B*, vol. 405, no. 10, pp. 2427–2430, 2010.

[26] T. Harada and K. Tsuda, "Magnetic phase transitions of $Mn_{3-x}Cr_xGaC$ ($0 \le x \le 0.5$)," *Journal of Magnetism and Magnetic Materials*, vol. 140, no. 2, pp. 135–136, 1995.

[27] T. Harada and K. Nishimura, "Transport properties of ternary magnetic compounds $Mn_{3-x}M_xGaC$ (M = Cr and Fe)," *Japanese Journal of Applied Physics*, vol. 32, no. 3, pp. 280–281, 1993.

[28] M. Nie, C. Wang, Y. C. Wen et al., "Magnetic phase transitions of antiperovskite $Mn_{3-x}Fe_xSnC$ ($0.5 \le x \le 1.3$)," *Solid State Communications*, vol. 151, no. 5, pp. 377–381, 2011.

[29] K. Motizuki and H. Nagai, "Electronic band structures and magnetism of the cubic perovskite-type manganese compounds Mn_3MC, (M = Zn, Ga, In, Sn)," *Journal of Physics C*, vol. 21, no. 30, article 5251, 1988.

[30] K. G. Efthimiadis, S. C. Chadjivasiliou, K. G. Melidis et al., "On the influence of Al on the magnetic ground state of 3d ferromagnetic alloys," *Journal of Magnetism and Magnetic Materials*, vol. 162, no. 2-3, pp. 259–264, 1996.

[31] Y. Wen, C. Wang, Y. Sun, G. Liu, M. Nie, and L. Chu, "Lattice, magnetic and electronic transport behaviors of Ge-doped Mn_3XC (X = Al, Zn, Ga)," *Journal of Alloys and Compounds*, vol. 489, no. 1, pp. 289–292, 2010.

[32] K. Kamishima, T. Goto, H. Nakagawa et al., "Giant magnetoresistance in the intermetallic compound Mn_3GaC," *Physical Review B*, vol. 63, no. 2, Article ID 024426, 6 pages, 2001.